Chapter VI
Conclusions and Future Scope

Chapter VI
Conclusions and Future Scope

6.1 Conclusions

This chapter summarizes all the experimental outcomes of MeV ions induced modifications in chitosan-based biodegradable matrices' properties. It contains a brief discussion about the significance of obtained results for the scope of future prospective.

In the present investigation, a systematic study on three different systems, particularly, (i) pristine polymer matrices of chitosan and chitosan-PEO blend (ii) electrolyte systems of chitosan and silver nitrate salt at different doping and (iii) polymer nanocomposites matrices of (a) chitosan-Ag NPs and (b) (chitosan-PEO blend)-Ag NPs with varying composition has been studied. The self-standing films were prepared *via* solution casting route. All these films were irradiated with carbon and nickel ion beam of MeV energy at the fluences of 1×10^{11} and 1×10^{12} ion/cm^2. Finally, these matrices were analyzed by XRD for structural analysis, FTIR spectroscopy for functional groups and chemical bond investigations, UV-Visible for optical properties, impedance measurement for dielectric, conductivity and relaxation investigations, SEM and AFM for surface morphology. The observed results are unique for carbon and nickel ion irradiation. The research findings contribute to the opportunity in the fields of biodegradable polymer science, solid polymer electrolytes, biodegradable hybrid nanocomposites, bandgap engineering, shielding of UV, and electromagnetic interference.

The XRD studies reveal the existence of PEO's spherulite crystalline domain; therefore, the CP blend's structural degradation is relatively hindered, whereas, substantial deterioration in crystallite size for chitosan is perceived. The crystallite size of chitosan and CP blend is found to be 110.7 Å and 48.45 Å; these values decreased to 26.6 Å and 41.03 Å due to irradiation effect, respectively. The diffraction peaks relevant to the silver nitrate salt were not perceived in the XRD spectra for electrolyte films, implying that there is no extant of surplus salt in the SPE. The diffraction peak corresponds to chitosan was suppressed and reformed to a broader one, which endorsed the host matrix's structural reformation because of salt-polymer interaction. XRD studies of polymer nanocomposites show that the crystallite size exhibits an increasing tendency with composition level and has a decreasing response with an increase in

fluence. The degree of amorphization of the nanocomposites matrices is significant for heavier ion with higher fluence.

The molecular vibrational study of pristine polymer, the interaction between macromolecules of chitosan and PEO polymeric blend, complexation between polymeric host and salt, composition dependence response of polymer nanocomposites assembly as well as fluence and electronic energy loss concerned impact of MeV ions were explored by FTIR spectroscopy. The ATR-FTIR spectra of post irradiated chitosan revealed a newer vibration mode at 1710 cm^{-1} attributed to carbonyl bond (C=O) vibrations. The successive shift of amide I mode to higher wavenumber is perceived. This approves the release of frozen water molecules because of SHIs assisted branching of an established intra-chain H-bond network between water molecules and –OH and $–NH_2$ groups. The suppressed intensity of 1149 and 1070 cm^{-1} modes indicating the opening of tetrahydropyran rings due to cleavage of C–O–C linkages. The overlapped stretching vibration of O–H and N–H evolved at 3346 cm^{-1} is considerably detracted.

Conversely, the absence of carbonyl band in the CP blend case reveals a mutual stabilizing effect due to the simultaneous involvement of both polymers' constitutional elements during the irradiation process. The concentration-dependent spectra of electrolytes show peak relocation, amendment in peak intensity, and broadening of vibrational modes with variation in salt doping. The silver nitrate's vital vibrational mode's deficiency endorsed salt's fair complexation in the host matrix. After irradiation, the degree of amorphization of the SPE matrices increases due to randomization and degradation of macromolecular chains. The Ag NPs concentration-dependent ATR-FTIR spectra of chitosan-Ag NPs reveal broadening and shifting some vibrational modes toward the lower wavenumber side with waning in peak intensity.

Similarly, dispersion of Ag NPs results in the broadening of the IR modes with lower wavenumber side shifting for the case of (chitosan-PEO)-Ag NPs assembly. Although, the peak intensity of 1060 cm^{-1} (C–O–C stretching), 1341 cm^{-1} (CH_2 wagging) and 842 cm^{-1} (CH_2 rocking) modes assigned to PEO is moderately changed concerning the assigned modes of CS. Moreover, the presence of Ag NPs in both the matrices has significant effects on stretching vibration and wagging mode of $–CH_2$. The polymeric assembly nanoparticles caused confining effects and constrained the interactions among main and side-chain functional groups. The

polymer nanocomposites matrices also reveal fluence-dependent response after irradiation. Predictably, an atomic ratio of hydrogen to carbon (H/C) for all the polymeric systems was declined due to MeV ions irradiation. Also, the structural degradation of macromolecular occurred *via* rupture of numerous polymeric linkages and the formation of low-molecular species in association with the degassing of some volatile products.

The optical properties of the different polymeric assembly amended due to ion–polymer interactions are shown in Figure 6.1. For chitosan and CP blend matrices, the differential absorbance at 370 nm wavelength appreciably intensified. Also, absorption of the peak evolved at 310 nm noticeably elevated. This is evidence of establishing the color responsive resonating

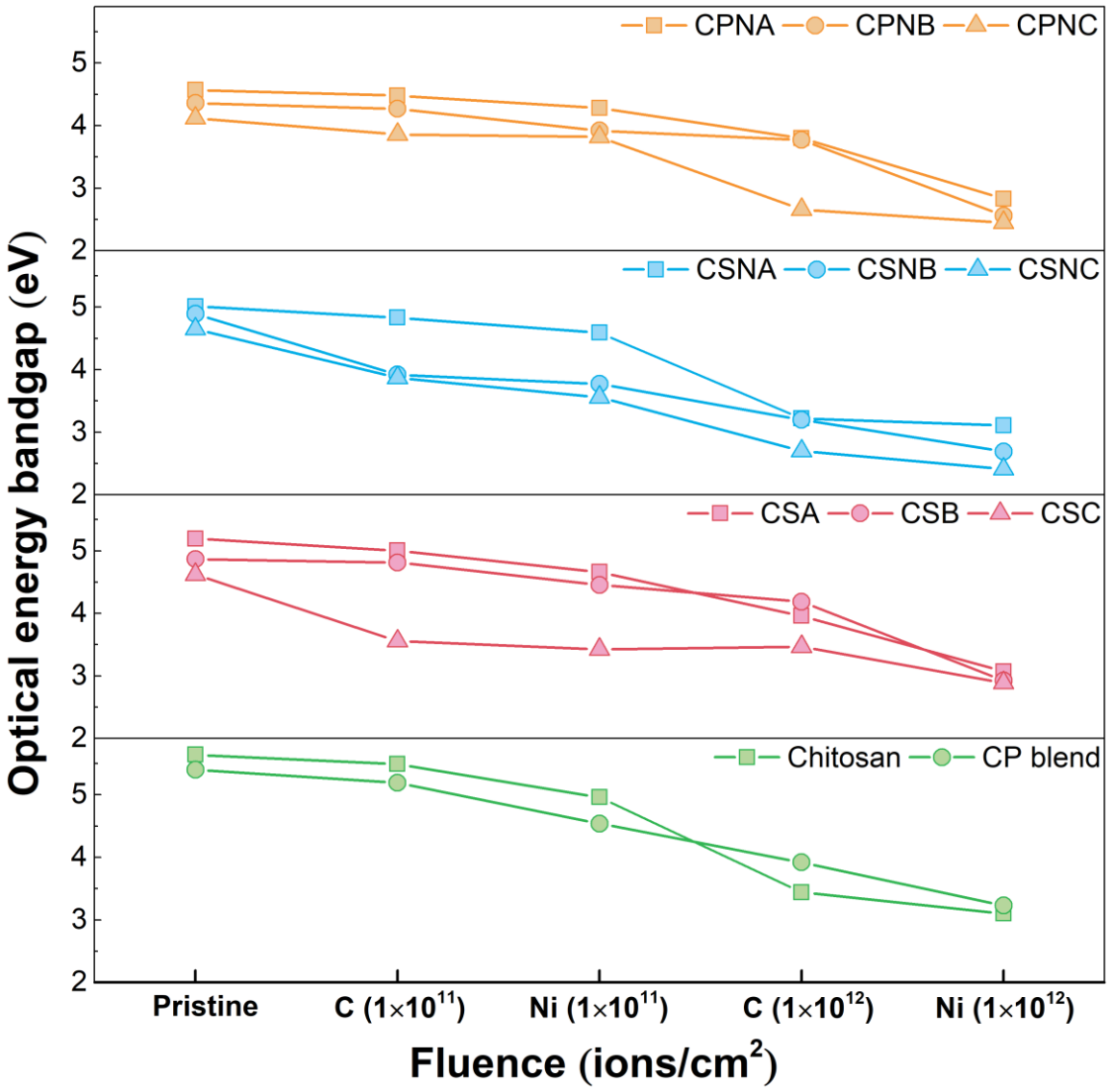

Figure 6.1 Optical energy bandgap of chitosan, CP blend, SPE and polymer nanocomposites matrices as a function of beam parameters.

matrix due to the formation of C=O, C=C and C=NH conjugated linkages. The presence of chromophores is responsible for the color transformation of the matrices. The SPE matrices' concentration-dependent response shows a well-resolved peak at 428 nm, indorse to the SPR of silver nanoparticles. The SPR peak intensity shows S_e and fluence-dependent response. The findings reveal Ag^+ ions' transformation into metallic Ag^0 nanoparticles *via* the static charge transfer process upon MeV ions irradiation. The Ag NPs concentration-dependent absorption spectra of chitosan-Ag NPs and (chitosan-PEO)-Ag NPs matrices exhibit the SPR peak around 410 nm. The SPR peaks are broader and have an asymmetric shape with a prolonged tail towards the higher wavelength regime. The SPR peak response indicates multipolar excitations and radiative damping due to elevated concentration of Ag NPs with variable-sized dispersion. Upon SHIs irradiation, in general, the AE exhibited a successive shift from the UV region to the visible region along with reformed shape. The red shift of AE ascribes the raise in charge carriers density, whereas ions induced defects are responsible for an improved profile. These modifications may ease the excitation of non-bonding electrons from the valance band to the conduction band. As a result, the optical band gap reasonably waned. The variation of E_g with beam parameters for all the polymeric system is depicted in Figure 6.1. The modification by 60 MeV C^{+5} is relatively different than that of 100 MeV Ni^{+7} irradiated films. By varying the beam parameter, the values of E_g of is successfully engineered is attributed to the formation of new energy levels (traps) between the HOMO and LUMO band. The waning in bandgap also suggested dropping the H/C atomic ratio, thereby promoting the carbonaceous clustering due to sp^3 to sp^2 hybridization. The condensation of carbon atoms clustering is found superior for excess electronic energy loss with higher fluence.

Frequency-dependent dielectric constant shows low-frequency dispersion response, whereas corresponding values at higher frequency domain attained relatively lower value. Indeed, the lower frequency window's response indorses the origination of the electrical double layer (i.e. space charge/interfacial polarization) at the interface of polymer and electrode boundaries due to the accumulation of charge carriers. The dielectric constant across the entire range of frequency is enhanced with increasing composition and fluence (See Figure 6.2). SHIs induced low-frequency abrupt rise in dielectric constant indorse values to the branching of polymeric main and side chains. While the increased dielectric constant at the higher frequency domain shows an increase in charge carriers density. The dielectric loss spectra reveal exponent response, obeying the relation, $\varepsilon'' \propto f^{-1}$, with the absence of loss peak. It exhibits an abrupt rise

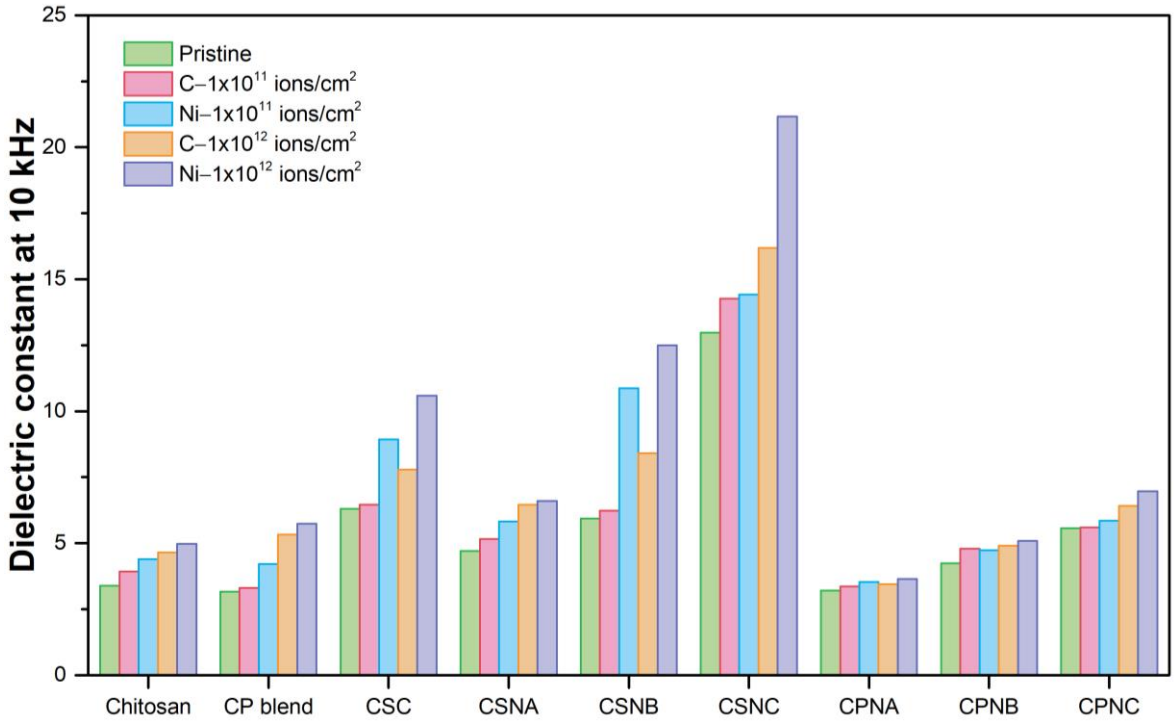

Figure 6.2 Dielectric constant at 10 kHz frequency of chitosan, CP blend, SPE and polymer nanocomposites matrices as a function of beam parameters.

at low-frequency window (f <1 kHz), whereas attained lower values at the high-frequency window (f >1 kHz), indicating the prevailing contribution of polarization effect over the dc conductivity. The dielectric loss increases with an increase in additive level and ion fluence.

In modulus analysis, the real modulus response upon SHIs irradiation shows diminishing response across the broad frequency range. It reveals ease of segmental, side chain, and charge carriers' mobility because of a decrease in the rigidity or moment of inertia of polymeric chains. The imaginary modulus spectra reveal a well-resolved relaxation peak. The relaxation peak shifted towards the regime of high frequencies window as a function of ion fluence. The values of shape parameters obtained from the Bergman fit depict a non-Debye type relaxation phenomena. The shape parameter's lower values infer the non-exponential nature of relaxation dynamics, and the charge carriers movement is a cooperative event with segmental motion.

Pristine and irradiated polymeric systems under study depict universal dielectric response and the frequency exponent "s" varying in between zero and one. Also, the frequency-dependent conductivity enhances after the irradiation. Improved DC conductivity suggests that disrupted crystallinity upon MeV ions irradiation might ease charge carriers' transportation through the

amorphous phase. The rise in AC conductivity is attributed to enhance charge carriers density, chain scission, unsaturation, and established carbon-rich network. The scaling study shows that the relaxation and conduction process is independent of MeV ions irradiation.

The surface feature of the polymeric system is substantially reformed concerning the composition and beam parameters. An amendment in morphological properties is explored using AFM and SEM analysis. The surface becomes relatively irregular due to additive involvement, whereas, MeV ions exposer promotes remarkably flatter and smoother morphology. The Ni^{+7} ions authentically cause a more significant impact due to somewhat higher S_e value and heavier mass. The suppression of nodules and knots implies an increased degree of an amorphous phase.

6.2 Future Scope

Plenty of advanced research on various perspectives is viable to study the ultimate interest including pragmatic device-based applications. In the current study, high energetic ions induced modifications in the properties of the unary, binary, and ternary polymer system based on chitosan, PEO, and silver. These systems can be optimized with distinctive blending and suitable additives. The future scope and work plan base on the present investigation are mentioned below:

- Synthesis of chitosan and CP blend based hybrid matrices incorporated with SnO_2, TiO_2 and ZnO, and the decorated carbon nanotube with SnO_2, TiO_2 and ZnO followed by gamma and MeV ions irradiation. Irradiation induced modifications in optical, luminescence, dielectric, and gas sensing properties will be investigated.
- Synthesis of chitosan and CP blend base SPE with metal salts, namely, $Cu(NO_3)_2$, $Ni(NO_3)_2$, and $AuCl_3$, followed by gamma, proton, and carbon ions irradiation to explore the optical, electrical, and antibacterial properties.
- In situ residual gas analysis will be performed during the irradiation to understand the degradation mechanism. Positron annihilation spectroscopy will also be implemented for the pristine and irradiated samples to understand free volume theory's role to insight the irradiation induced physicochemical and dielectric responses.